Received: 3 April 2020 | Revised: 14 May 2020 | Accepted: 21 May 2020

DOI: 10.1002/jmor.21222

RESEARCH ARTICLE

Journal of morphology WILEY

The denticle surface of thresher shark tails: Three-dimensional structure and comparison to other pelagic species

Meagan Popp[1] | Connor F. White[1] | Diego Bernal[2] | Dylan K. Wainwright[1] | George V. Lauder[1]

[1]Department of Organismic and Evolutionary Biology, Harvard University, Cambridge, Massachusetts

[2]Department of Biology, University of Massachusetts Dartmouth, Dartmouth, Massachusetts

Correspondence
George V. Lauder, Museum of Comparative Zoology, 26 Oxford Street, Cambridge, MA 02138.
Email: glauder@oeb.harvard.edu

Funding information
National Oceanic and Atmospheric Administration, Grant/Award Number: NA16NMF4270231; National Science Foundation, Grant/Award Numbers: IOS-1354593, GRF DGE-1144152; Office of Naval Research, Grant/Award Numbers: N00014-09-1-0352, N000141410533

Abstract

Shark skin denticles (scales) are diverse in morphology both among species and across the body of single individuals, although the function of this diversity is poorly understood. The extremely elongate and highly flexible tail of thresher sharks provides an opportunity to characterize gradients in denticle surface characteristics along the length of the tail and assess correlations between denticle morphology and tail kinematics. We measured denticle morphology on the caudal fin of three mature and two embryo common thresher sharks (*Alopias vulpinus*), and we compared thresher tail denticles to those of eleven other shark species. Using surface profilometry, we quantified 3D-denticle patterning and texture along the tail of threshers (27 regions in adults, and 16 regions in embryos). We report that tails of thresher embryos have a membrane that covers the denticles and reduces surface roughness. In mature thresher tails, surfaces have an average roughness of 5.6 μm which is smoother than some other pelagic shark species, but similar in roughness to blacktip, porbeagle, and bonnethead shark tails. There is no gradient down the tail in roughness for the middle or trailing edge regions and hence no correlation with kinematic amplitude or inferred magnitude of flow separation along the tail during locomotion. Along the length of the tail there is a leading-to-trailing-edge gradient with larger leading edge denticles that lack ridges (average roughness = 9.6 μm), and smaller trailing edge denticles with 5 ridges (average roughness = 5.7 μm). Thresher shark tails have many missing denticles visible as gaps in the surface, and we present evidence that these denticles are being replaced by new denticles that emerge from the skin below.

KEYWORDS

caudal fin, elasmobranch, locomotion, scale, skin

1 | INTRODUCTION

Despite the remarkable ecological and morphological diversity of sharks, all species share a unique morphological feature: skin covered with small dermal denticles or placoid scales. Shark denticles have a tooth-like structure with an enameloid and dentine outer layer and an inner pulp cavity. Denticles are complexly shaped with a flattened outer crown area that is connected to narrower neck that extends toward the skin and an expanded base embedded in the dermis (Ankhelyi, Wainwright, & Lauder, 2018; Castro, 2011; Díez, Soto, & Blanco, 2015; Motta, Habegger, Lang, Hueter, & Davis, 2012; Oeffner & Lauder, 2012; Rangel, Amorim, Kfoury, & Rici, 2019; Reif, 1982).

Although in recent years both interspecific and intraspecific diversity of denticle shape and size have been studied, there is still little

consensus on the relationship between specific morphological features of denticles and their function as skin surface structures (Lauder et al., 2016; Lauder & DiSanto, 2015). Various functions of denticles have been suggested, including protection from parasites and abrasion (Raschi & Tabit, 1992), defense (Raschi & Tabit, 1992), focusing bioluminescent signals (Reif, 1985b), and even holding prey against the body during feeding (Southall & Sims, 2003). Substantial effort has also been directed toward studying the hydrodynamic properties of denticles which have been proposed to include both drag reduction (Bechert, Hoppe, & Reif, 1985; Fernandez-Waid et al., 2019; Lang, Motta, Hidalgo, & Westcott, 2008; Reif, 1985a), and lift and thrust enhancement (Domel et al., 2018; Oeffner & Lauder, 2012; Wen, Weaver, & Lauder, 2014). Hydrodynamic testing of flexible and rigid foils covered with 3D-printed biomimetic denticles has provided a better understanding of shark skin hydrodynamics (Domel et al., 2018; Domel, Saadat, et al., 2018; Wen, Weaver, Thornycroft, & Lauder, 2015), but we still lack an understanding of how denticle morphology is related to the flow regime on different areas of the shark body surface.

One approach to this issue is to measure differences in skin denticle structure and surface characteristics that can be associated with clearly-identifiable differences in skin motion. If, for example, it is possible to correlate denticle surface features with the amplitude of body or tail motion, both within individuals and among species, this could provide a window into structure–function relationships of the skin surface in sharks.

The unique tail of thresher sharks (Alopiidae) provides an opportunity to examine skin surface features in relationship to movement patterns (Frumkin & Shimada, 2020). Thresher sharks are potentially useful for testing hypotheses of denticle structure and function because of the considerable length of their tail, which comprises up to 50% of an individual's total length (Castro, 2011; Smith, Rasmussen, Ramon, & Cailliet, 2008) and exhibits a substantial gradient in undulatory amplitude during swimming. The base of the thresher shark tail moves in an oscillatory manner with amplitude similar to most other shark species, but the tip of the elongated tail is extremely flexible and exhibits high amplitude undulation even during steady swimming (Aalbers, Bernal, & Sepulveda, 2010). It is reasonable to hypothesize that differences in tail oscillation amplitude will be correlated with changes in skin surface characteristics, perhaps involving a gradient along the tail length in denticle size, ridge number, or overall skin surface roughness.

Thresher sharks also utilize their highly elongate tail to immobilize prey with a slap-like motion, pitching the tail over their head and striking individual fish in a school (Aalbers et al., 2010; Frumkin & Shimada, 2020; Oliver, Turner, Gann, Silvosa, & D'Urban, 2013; Preti, Smith, & Ramon, 2001; Smith et al., 2008). Field observations and published video of the tail strike clearly show a gradient of undulatory tail motion, from the tail base toward the extreme movements exhibited by the tail tip (Oliver et al., 2013). The unique function of the thresher caudal fin in predatory strikes may be associated with novel skin surface structures.

The goals of this paper are first, to provide a comprehensive description of three-dimensional surface roughness characteristics of the tail surface of mature thresher sharks using surface profilometry (Ankhelyi et al., 2018; Wainwright & Lauder, 2016; Wainwright, Lauder, & Weaver, 2017). Surface profilometry allows quantification of denticle morphology in three dimensions, and we present data both spanwise along the tail length, and chordwise from leading to trailing edge at several locations along the span to provide a comprehensive description of thresher shark tail denticle diversity. Second, we use both surface profilometry and histology to compare the three-dimensional structure of tail denticles in embryo and mature thresher sharks. Because the tail of embryonic thresher sharks has never been used for feeding or locomotion, it can reveal ontogenetic changes in denticle structure and function. Third, we compare surface metrics of denticle morphology in thresher sharks to caudal fin denticle characteristics for 11 other oceanic shark species. Fourth, we use scanning electron microscopy to describe several of the novel features of the denticle surface discovered in thresher shark tails. Finally, we evaluate a specific hypothesis relating denticle structure to tail function. We hypothesize that tail surface roughness should increase from the base of the tail toward the tip due to increased undulation and oscillation amplitude of the tail tip. If skin surface roughness is correlated with swimming function, then we expect regions of greater tail undulation to possess increased surface roughness due to the likely increase in flow separation as oscillation amplitude increases. An increase in tail surface roughness could reduce separation by "tripping" the boundary layer from laminar to turbulent toward distal tail regions (Schetz, 1993; Schlichting, 1979).

2 | MATERIALS AND METHODS

2.1 | Study animals and skin sampling

Tails were obtained from three mature thresher sharks (*Alopias vulpinus* Bonnaterre, 1788). Specimens were collected by rod and reel (National Marine Fisheries Scientific Permit #HMS-SRP-18-04 (n = 2) off shore of Massachusetts, USA, while a third tail was collected from a mature individual obtained during a biodiversity survey by the US National Marine Fisheries Service (NOAA, n = 1) off shore of San Diego, California USA. The tails of two embryo thresher sharks were obtained from off shore of San Diego, California USA. The tails of all three mature individuals were removed from the body at approximately 90% of fork length and kept frozen until sampled as described below. No significant damage had been done to any of the tails and all were treated with special care to avoid damaging the skin. The lengths of the three tails (from base of the caudal peduncle to the tail tip) were 165, 172, and 191 cm. Additionally, the tails of two embryo common thresher sharks (obtained under CDFW Scientific Collecting Permit #3450) used in this study had lengths of 66 and 70 cm.

Comparative denticle morphology data from the tails of 11 other species were obtained from specimens belonging to the Harvard Museum of Comparative Zoology's (MCZ) Ichthyology collection, as well as additional specimens obtained by the authors that were frozen or stored in 70% ethanol. These additional specimens will be

deposited in to the MCZ Ichthyology collection when other ongoing studies are completed. Surface profilometry data were obtained from these comparative species at a location approximately midway between the caudal peduncle and the tip of the tail (i.e., location #18 in Figure 1b). The 11 comparative species were: a white shark (*Carcharodon carcharias*, stored in 70% ethanol, MCZ Ichthyology #171013), a shortfin mako shark (*Isurus oxyrinchus*, collected under Scientific Permit #HMS-SRP-18-04, frozen), two bonnethead sharks (*Sphyrna tiburo*, frozen), two blacktip shark tails (*Carharhinus limbatus*, frozen), one silky shark (*Carcharhinus falciformis*, stored in 70% ethanol, MCZ Ichthyology # 40787), one porbeagle (*Lamna nasus*, frozen), one leopard shark (*Triakis semifasciata*, stored in 70% ethanol), one blue shark (*Prionace glauca*, stored in 70% ethanol, MCZ Ichthyology #36035), one spiny dogfish (*Squalus acanthias*, stored in 70% ethanol), one basking shark (*Cetorhinus maximus*, stored in 70% ethanol, MCZ Ichthyology #54413), and three smooth dogfish (*Mustelus canis*, frozen) at Harvard University.

Skin samples were taken from 27 regions on the three mature thresher tails and 16 regions on the two embryo thresher tails (Figure 1). Most of the regions of interest correspond to the leading edge, middle surface, and trailing edge at various span positions along the tail length. We define tail span here as the distance from the center of the caudal peduncle (or base of lower lobe) at the location of the anterior edge of the precaudal pit to the tip of the tail. Thresher sharks have a notch-like depression on the dorsal and ventral surfaces of the caudal peduncle just anterior to the dorsal and ventral caudal fin lobes that is referred to as the precaudal pit. Samples were taken at span measurements of 10, 30, 50, 70, and 90% along the dorsal lobe of the tail while samples from the ventral (hypochordal) lobe were taken at the 50% span location (Figure 1). Samples were oriented with their top and bottom edges parallel to the horizontal body axis (Figure 1c) and were cut larger than the region subsequently imaged to avoid edge effects when imaging. Each skin sample was approximately 5 × 5 cm on each side (some samples near the leading and trailing edges were smaller than this) and 2 mm thick. The grey area in Figure 1c shows the sample removed, while the inner white box schematically shows the region imaged using surface profilometry. The posteroventral corner of each sample was cut (Figure 1c) to indicate this direction and allow for sample orientation after removal.

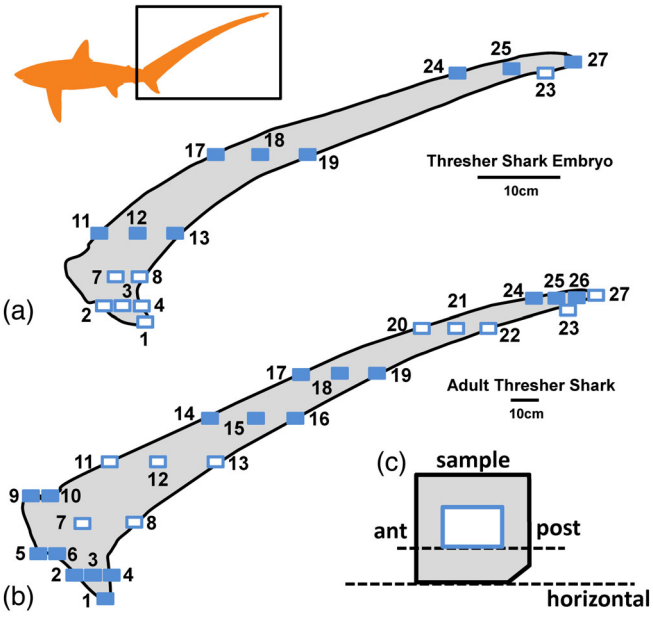

FIGURE 1 Sampling locations on the tails of *Alopias vulpinus* (a) embryo (n = 2) and (b) adult (n = 3) specimens; tail outlines are traced from one representative tail each. Numbers correspond to a specific sampled region on the tail and regions consist of leading edges, middle surfaces, and trailing edges (see Tables 1 and 2). Additional groupings are based on different percentage span distances along the tail from base to tip, including 0, 10, 30, 50, 70 and 90% on mature tails, along with other areas of interest. More precise information on sample locations is given in the Methods. Panel (c) shows the method for collecting rectangular skin samples allowing for the identification of the horizontal axis and posteroventral direction: ant, anterior; post, posterior; the notch is cut to indicate the posteroventral direction after sample removal. White area indicates the approximate region used for surface profilometry. Filled blue boxes indicate samples that appear as surface profilometry images in Figures 2, 3 and 9

Scanning electron microscopy samples were taken from one of the mature thresher shark tails at the leading edge at 50% span (region #17, Figure 1b), middle surface at 50% span (region #18, Figure 1b), and the trailing edge at 50% span (region #19, Figure 1b).

On mature common thresher individuals, sample locations were as follows (Figure 1b): the tip of the hypochordal lobe (region #1), leading edge of the hypochordal lobe at 50% span (region #2), middle surface of the hypochordal lobe at 50% span (region #3), trailing edge of the hypochordal lobe at 50% span (region #4), anterior to the ventral precaudal pit (region #5), posterior to the ventral precaudal pit (region #6), middle surface of the tail along a line of the horizontal body axis projected through the peduncle (region #7), trailing edge of the tail along a line of the horizontal body axis projected through the peduncle (region #8), anterior to the dorsal precaudal pit (region #9), posterior to the dorsal precaudal pit (region #10), leading edge at 10% span (region #11), middle surface of the tail at 10% span (region #12), trailing edge of the tail at 10% span (region #13), leading edge of the tail at 30% span (region #14), middle surface of the tail at 30% span (region #15), trailing edge of the tail at 30% span (region #16), leading edge of the tail at 50% span (region #17), middle surface of the tail at 50% span (region #18), trailing edge of the tail at 50% span (region #19), leading edge of the tail at 70% span (region #20), middle surface of the tail at 70% span (region #21), trailing edge of the tail at 70% span (region #22), subterminal lobe (region #23), leading edge of tail at 90% span (region #24), middle surface of the tail at 90% span (region #25), trailing edge of the tail at 90% span (region #26), and tip of the tail (region #27).

Surface profilometry samples from the thresher embryos were taken as follows, and sample numbers from embryos and mature individuals correspond roughly to homologous tail locations (Figure 1a): the tip of the hypochordal lobe (region #1), leading edge of the hypochordal lobe at 50% span (region #2), middle surface of the

hypochordal lobe at 50% span (region #3), trailing edge of the hypochordal lobe at 50% span (region #4), middle surface of the tail along the central body axis (region #7), trailing edge of the tail along the central body axis, (region #8), leading edge of the tail at 10% span (region #11), middle surface of the tail at 10% span (region #12), trailing edge of the tail at 10% span (region #13), leading edge of the of the tail at 50% span (region #17), middle surface of the tail at 50% span (region #18), trailing edge of the tail at 50% span (region #19), subterminal lobe (region #23), leading edge of the tail at 90% span (region #24), middle surface of the tail at 90% span (region #25), and tip of the tail (region #27). The membrane covering the denticles on these samples was removed prior to imaging with surface profilometry. In addition to these regions, six additional samples were taken with the surface membrane intact from the middle tail surface at 20% span, middle tail surface at 50% span, and middle tail surface at 90% span. Following surface profilometry with the membrane intact, the covering membrane was removed and the same regions were imaged again (Figures 8 and 9).

2.2 | Gel-based surface profilometry

Surface profilometry samples were obtained by removing patches of skin from two mature thresher tails. We subsequently obtained a handheld surface profilometry device that was used for the third mature specimen and removal of skin samples was not needed. Handheld surface imaging was also used for several of the tails from the 11 comparative species studied. Gel-based surface profilometry (Johnson & Adelson, 2009; Wainwright et al., 2017, 2019; Wainwright & Lauder, 2016) does not require any specimen preparation. Selected samples from frozen specimens were thawed and imaged directly without being preserved.

The gel based profilometry technique (GelSight Incorporated, Waltham, MA) was used to quantify skin surface metrology variables and describe three-dimensional (3D) skin surface structure following our previous methodology (Ankhelyi et al., 2018; Domel, Domel, et al., 2018; Wainwright et al., 2017, 2019; Wainwright & Lauder, 2016). Gel-based profilometry involves pressing a deformable clear gel elastomer (with one opaque, coated surface) onto an object. The coated surface of the gel conforms to the object, and a series of six photographs are taken with different illumination angles. Once the images are processed, a 3D-image of the surface is reconstructed to create a topographical representation of that surface. This surface profilometry approach has been validated in our previous research with known standards and used in the past to image other shark species, several bony fish species, cetacean skin, and other materials with known surface structure (Ankhelyi et al., 2018; Baeckens, Wainwright, Weaver, Irschick, & Losos, 2019; Wainwright et al., 2017, 2019).

We imaged 27 regions from each mature thresher shark and 16 regions from each embryo specimen (Figure 1) using the surface profilometry technique, and then processed the 3D-surfaces using MountainsMap (v. 7 Digital Surf, Besançon, France). In MountainsMap software, large-scale background curvature was removed from each surface and then several metrology variables were calculated from the de-trended data matrix for each sample following the procedures outlined in Ankhelyi et al. (2018). Surface metrology variables using three-dimensional coordinates included roughness (Sq), skew (Ssk), kurtosis (Sku), and maximum height (Sz). These variables were calculated for each sample on each of three mature thresher tails and the two embryo tails. We also measured the average length, average width, and average aspect ratio (length to width ratio) of three denticles for every region in each individual, as well as the spacing between adjacent denticle ridges (where present) and denticle ridge height (height above the denticle crown valleys) for three denticles in each region. Roughness (Sq) values (in μm) are calculated by taking the squared distance of each point from the mean height and then calculating the square-root of the sum across that surface. Wainwright and Lauder (2016) and Wainwright et al. (2017)) provide further discussion of calculated variables. Both skew (Ssk) and kurtosis (Sku) variables describe distribution of height across the surface. A surface with a normal distribution of height will have a Ssk of zero and a Sku of three (mesokurtic). Surfaces with positive Ssk are characterized by more peaks, and surfaces with negative skew are characterized by relatively greater numbers of valleys. Kurtosis values above three indicate surfaces with low valleys and high peaks (leptokurtic), while Sku values below three indicate that surface variation is less extreme (platykurtic; Dotson, 2015; Raghavendra & Krishnamurthy, 2013; Westfall, 2014). Maximum height (Sz) of the surface, measured in μm, is the maximum height measured from the lowest point of the sample.

Isotropy is measured using an autocorrelative function and distinguishes isotropic surfaces from anisotropic surfaces. Anisotropic surfaces have directional patterns (values close to 0%), while isotropic surfaces have no privileged direction (values near 100%). Texture direction is measured by the directionality of the dominant direction of the surface. We also measured angles (using MountainsMap software) from the horizontal axis to show the directionality of surface ridges on denticles.

To provide context for shark tail roughness values, three-dimensional surface samples were measured using gel-based profilometry for several other common materials as well as competition swim suit surfaces and these data are discussed in the supplemental document and supplemental Table S1.

2.3 | Histology

We found that the tails of embryo thresher sharks were covered in a thin membrane. To assess the relationship between this surface membrane and underlying denticles we removed one sample from the middle tail surface at 50% span (region #18, Figure 1a) and processed it for histological analysis. This sample was cut into several smaller 1 mm square portions that were then fixed in paraformaldehyde, embedded in paraffin resin, processed into 10-μm thick slices, and then stained with hematoxylin and eosin. Images of the prepared slides were taken with a Leica DM 2500 P compound microscope (Leica Microsystems, Wetzlar, Germany) under either ×103 or ×203 magnification.

2.4 | Data analysis and statistics

Analysis followed the approach used by Wainwright and Lauder (2016) and Ankhelyi et al. (2018) for similar profilometry data for fish and sharks. All analyses were conducted using the statistical software R (R Foundation for Statistical Computing, Vienna, Austria). First, a correlation matrix for each data set, including data only from the dorsal tail lobe, was calculated to determine which variables were highly correlated (with a cutoff of above 0.65 or below −0.65) with each other. A subset of variables (see below) was then chosen to include only one within any group of highly correlated variables. Second, three separate Multivariate Analysis of Variance (MANOVA) tests were used to identify significant differences within the leading edge, middle surface, and trailing edge surfaces of tail denticles, the span (distance along the tail) percentage, and between mature and embryo tails. Variables included in the MANOVA analysis for the leading edge, middle surface and trailing edge and span percentage profilometry data were Sq, Ssk, mean length, aspect ratio (AR), isotropy, texture direction 1, angle from the horizontal axis, and mean ridge height. Third, separate ANOVAs were then conducted with the categorical variable body regions as the independent variable for each trait to determine which variables contributed to the overall significance of each MANOVA. Fourth, Tukey HSD post hoc tests were conducted on each variable with p-values less than .05 from the ANOVA to determine the statistical grouping of the different body regions for each variable. Finally, three discriminant function analyses (DFA) were conducted on the surface profilometry data. The DFAs mirrored the MANOVAs and included the continuous variables and categorical groupings (leading/middle/trailing edges, span percentage of the dorsal tail lobe, and mature vs. embryo) used in each MANOVA and given above. These DFAs allowed us to display the between-group variance in each comparison and better understand what variables help most in distinguishing denticle morphology among different groups.

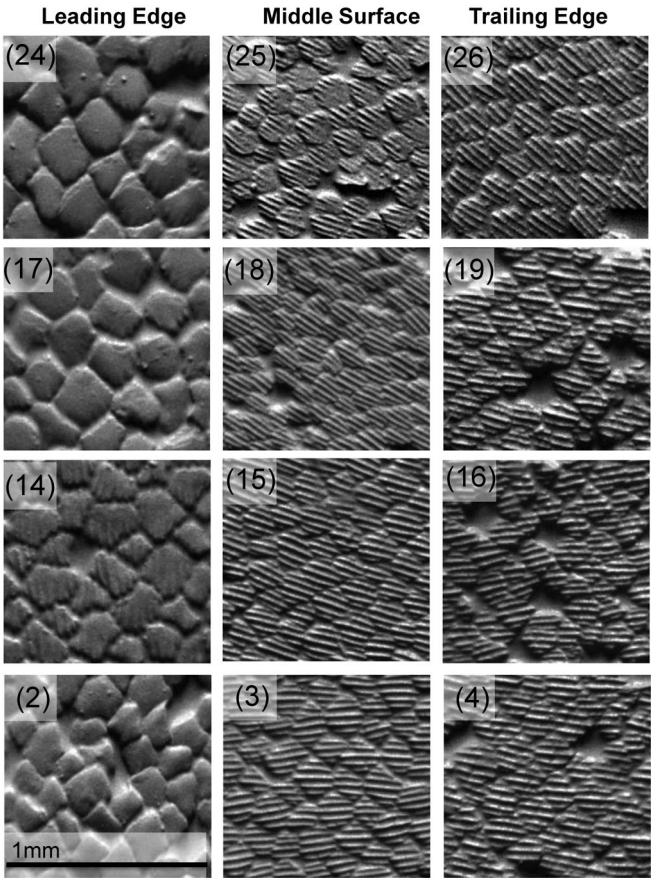

FIGURE 2 Images (obtained using surface profilometry, see Methods) of mature thresher shark tails to demonstrate denticle diversity on different regions of the caudal fin. Panels are labeled by the assigned number corresponding to the locations in Figure 1b. Additional locations are shown in Figure 3. Measurements of surface characteristics are given in Table 1. Note missing denticles in several of the images. Scale bar refers to all panels. Anterior is to the left for middle and trailing edge samples; anterior is down for leading edge samples

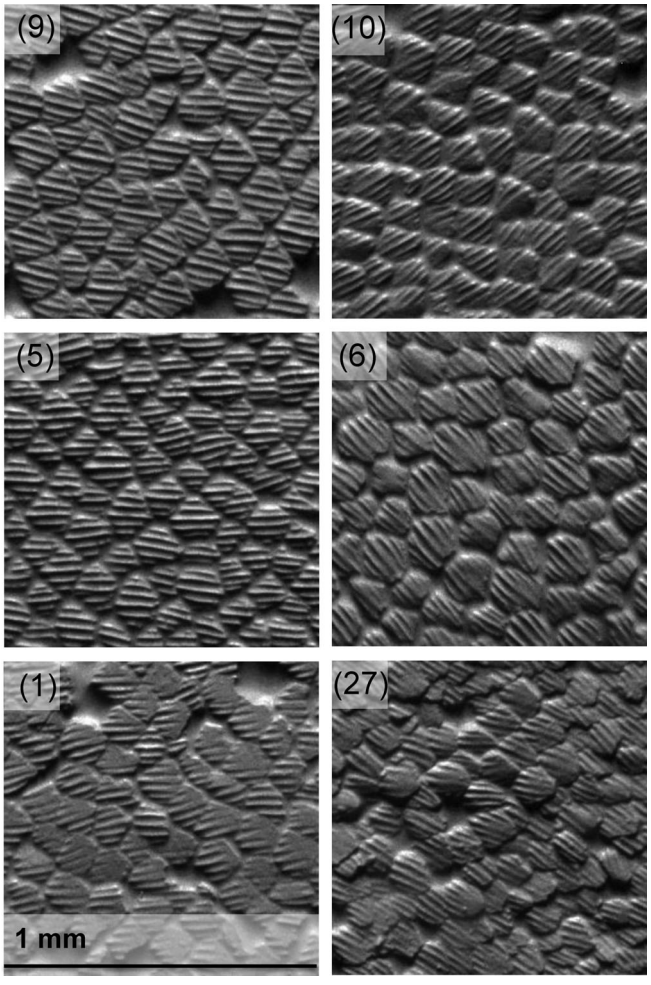

FIGURE 3 Images (obtained using surface profilometry, see Methods) of mature thresher shark tails showing additional sample locations to those illustrated in Figure 2. Panels are labeled by the assigned number corresponding to the locations in Figure 1b. Measurements of surface characteristics are given in Table 1. Scale bar refers to all panels; anterior is to the left for all images

TABLE 1 Profilometry measurements for skin samples from mature thresher sharks (*Alopias vulpinus*)

Named region	Sample number	Sq (μm)	Ssk	Sku	Sz (μm)	Isotropy	Texture direction 1 (°)	Denticle length (μm)	Denticle width (μm)	Ridge height (μm)	Ridge spacing (μm)	Angle from Horiz. Axis (°)
Ventral tip	1	10.9	−1.1	7.0	108	79	10	193	202	2.4	28	12
V50% lead	2	8.9	−0.4	3.4	58	71	−20	292	205	0	NA	3
V50% mid	3	6.4	−1.1	7.5	55.	74	−5	180	168	4.4	38	7
V50% trail	4	6.3	−0.9	5.5	63	84	0.1	184	177	5.9	42	8
V anterior precaudal pit	5	5.5	−0.4	3.5	38	85	0.1	195	170	4.9	43	11
V posterior precaudal pit	6	6.5	−0.5	3.4	45	65	26	225	207	5.1	40	21
Central mid	7	5.4	−0.6	4.2	35	67	10	187	193	5.5	45	13
Central trail	8	8.3	−0.6	4.0	62	79	18	164	156	5.5	42	10
D anterior precaudal pit	9	5.8	−0.7	5.4	45	65	−10	193	206	4.2	42	13
D posterior precaudal pit	10	5.8	−0.3	3.2	40	77	−35	167	176	3.6	37	14
D10% lead	11	9.5	−1.2	7.0	97	85	−35	146	220	4.3	45	32
D10% mid	12	4.6	−0.7	4.9	36	71	36	178	153	4.2	40	19
D10% trail	13	4.0	−0.9	5.8	56	56	6	168	150	5.3	40	15
D30% Lead	14	7.5	−1.0	4.9	52	78	17	256	240	1.1	23	11
D30% mid	15	4.4	−1.2	7.5	39	78	26	173	149	4.2	35	30
D30% trail	16	5.1	−1.3	7.5	44	77	0.1	187	160	5.7	41	7
D50% lead	17	9.4	−0.7	4.2	67	85	53	249	227	0	NA	0
D50% mid	18	5.6	−1.4	9.8	63	78	25	174	151	2.5	33	30
D50% trail	19	6.7	−1.5	8.2	58	82	16	188	167	4.6	38	14
D70% lead	20	10.4	−0.7	5.1	103	81	54	287	233	0	NA	0.2
D70% mid	21	4.9	−1.8	13.8	51	84	30	172	145	3.1	32	31
D70% trail	22	6.9	−1.5	8.2	64	85	26	177	168	4.8	38	20
D lobe	23	6.6	−1.3	7.4	66	78	33	193	168	3.7	35	34
D90% lead	24	12.1	−1.1	8.1	112	81	−24	314	241	0	NA	11
D90% mid	25	6.4	−1.4	8.6	55	80	63	176	164	2.8	34	36
D90% trail	26	5.3	−1.3	6.6	40	82	34	182	182	3.4	37	34
Dorsal tip	27	8.0	−0.7	5.5	60	82	−5	219	195	1.7	37	30

Note: Values shown are means ($N = 3$ individuals, for metrics of surface roughness; $N = 3$ denticles from each of three individuals for the length, width, height and spacing measurements). Variation among locations is shown in Figure 11. Sample numbers (locations along the tail) are provided in Figure 1. Detailed variable descriptions are provided in the Methods section. NA indicates no ridge spacing when denticle ridges have zero height (i.e., ridges are absent).

Abbreviations: D, dorsal; lead, leading edge; lobe, subterminal lobe; mid, middle/lateral portion of the body; Sku, kurtosis; Sq, roughness; Ssk, skew; Sz, maximum feature height; tip, tip of the caudal fin; Trail, trailing edge; V, ventral.

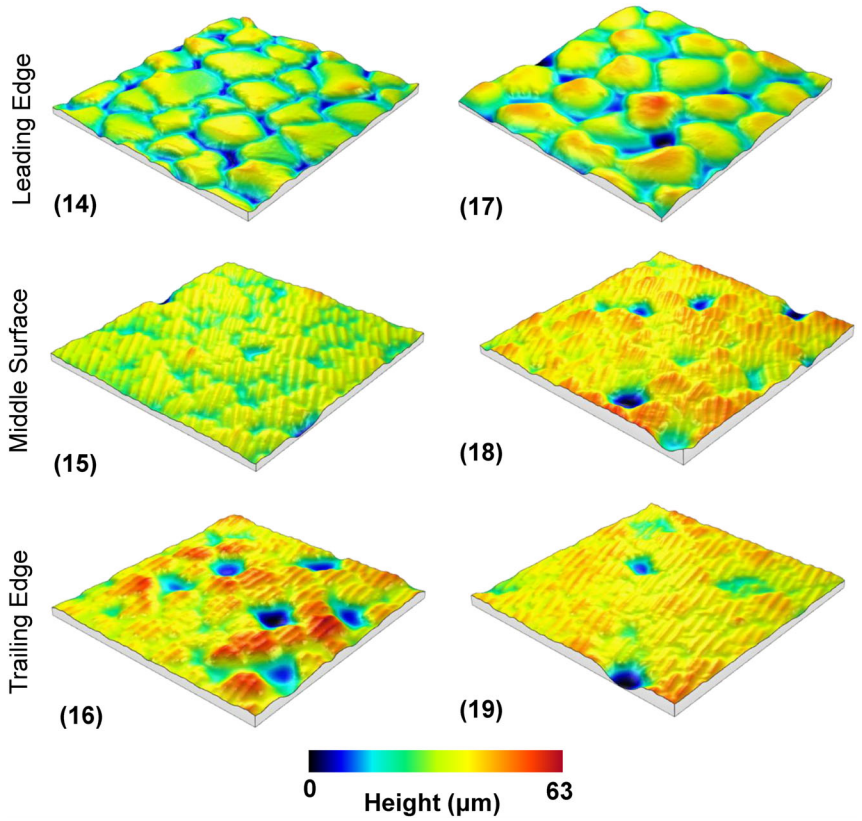

FIGURE 4 Three-dimensional surface profilometry images from mature thresher shark tails showing surface height variation. Color shows the height of the denticles: all panels are scaled to this same maximal height. Images are numbered corresponding to the sample scheme shown in Figure 1b. Images are 1 mm by 1 mm in size. Images with greater variation in red and blue coloring correspond to regions with increased surface roughness as reported in Table 1

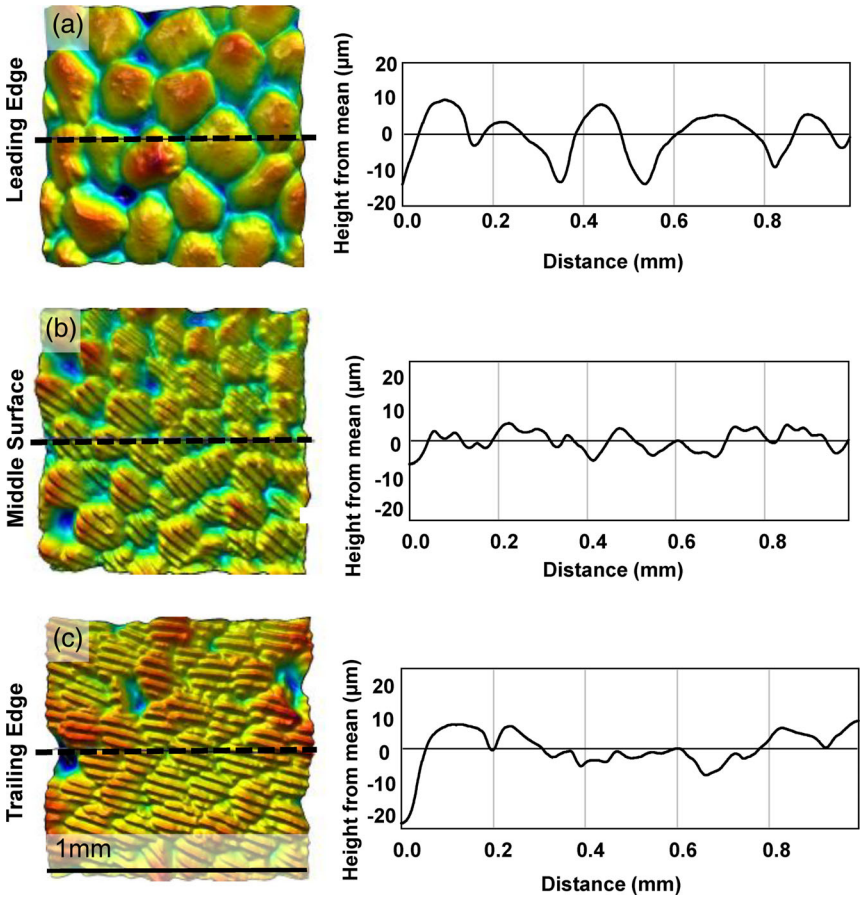

FIGURE 5 Surface profilometry analyses from selected samples of a mature thresher shark tail. Panel (a) corresponds to region #17, panel (b) to #18, and panel (c) to #19 (Figure 1b). Left column shows surface profilometry where color represents the height with red representing the maximum height of 55.5 μm, and blue the minimum height of −20.2 μm. For all panels in this figure, zero height is the mean surface height. Right column shows height profiles for each surface at the position indicated by the black line. All samples are 1 mm by 1 mm. Anterior is to the left for middle and trailing edge samples; anterior is down for leading edge samples

3 | RESULTS

3.1 | Adult thresher shark tail denticle morphology

Images of the denticle surface from 18 regions on the tail of mature thresher sharks (Figures 2 and 3) illustrate differences in denticle morphology, orientation, surface patterning and spacing. Denticles vary considerably in size and surface ridge orientation depending on the tail region in which they are located. Denticles at the leading edges of the tail possess flat crowns that lack ridges except near the base of the tail at location #11, and are larger in comparison to denticles at other tail regions. On the tail surface and trailing edge, denticles typically have five ridges. We also observed numerous gaps in the denticle surface at all tail locations where denticles appear to have been lost, creating a pit in the surface approximately the size of a single denticle (Figures 2 and 3).

Table 1 presents denticle data for the 27 sampled sites along the tail of mature thresher sharks. Denticle length in mature threshers varies from 314 μm at the leading edge at 90% span to 146 μm at the 10% span leading edge (Table 1). The leading edge has higher roughness values than the middle or trailing surfaces due to gaps separating adjacent denticles. Tail leading edge samples from the dorsal lobe have roughness values (9.8 μm) almost twice those of the middle and trailing edge regions (5.2 and 5.6 μm respectively; Table 1). Middle surface and trailing edge denticles have five ridges that range in height from 5.9 μm on the ventral 50% span trailing edge to 2.5 μm on the dorsal 50% span middle surface (Table 1). The space between the ridges on the denticle crowns ranges from 32 μm on the dorsal 70% span middle surface to 45 μm on the central middle tail surface (Table 1).

Changes in denticle spacing around the tail surface can be seen in the three-dimensional surface profilometry data (Figures 4 and 5).

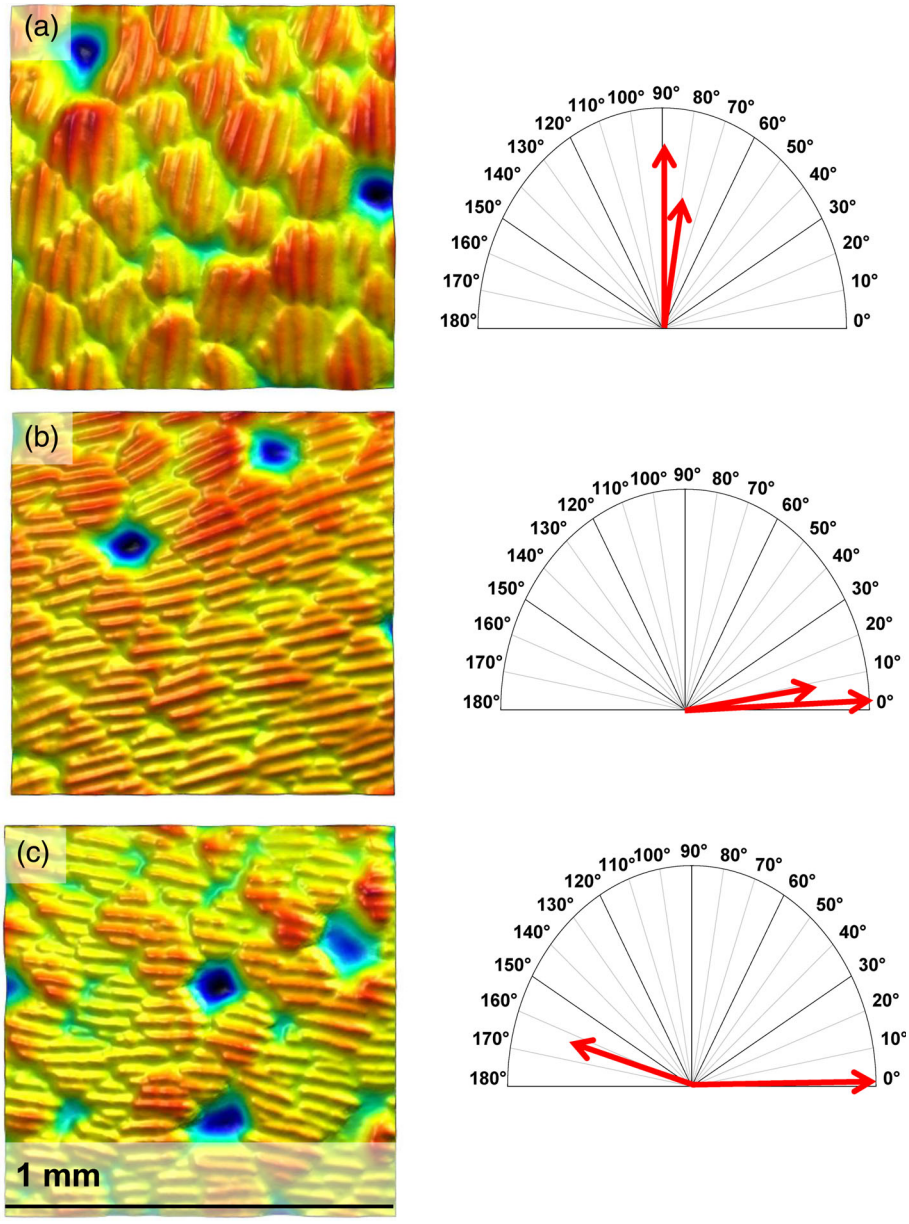

FIGURE 6 Surface profilometry images from a mature thresher shark individual to illustrate variation in texture direction; see Methods for a description of this measurement. Panel (a) is from region #11, panel (b) from region #12, and panel (c) from region #13 (Figure 1b). The left column shows surface profilometry images with color corresponding to surface height. Red represents the maximum height of 78 μm while blue corresponds to the minimum height of 0 μm. The right column shows the first and second texture directions (see Methods for details). The long arrow corresponds to the first principal direction, while the shorter arrow indicates the second principal direction. Direction angles are relative to the horizontal axis of 0° in all samples. Anterior is toward the bottom in panel (a) which is a sample at the leading edge of the tail base, while anterior is right for panels (b) and (c) which are tail surface samples

Transects showing surface height across the denticle surface (Figure 5) illustrate the greater variation present at the leading edge due to the larger, physically separated, denticles. Gaps in the denticle surface result in valleys that are at least 20 μm below mean surface height.

Analysis of surface texture direction (Figure 6) and measurement of denticle ridge angle relative to the horizontal body axis in lateral view (Table 1) illustrate variation in denticle ridge orientation around the tail surface. Most denticles have texture directions that are within 30° of the horizontal mid-lateral body axis (Table 1), but denticles at the 10% span location on the tail leading edge posterior to the transition from the caudal peduncle have ridges oriented parallel to sagittal plane, nearly at 90° to most other denticles (Figure 6a). Surface patterning on the mid-tail surface is oriented nearly horizontally (Figure 6b), while the trailing edge surface pattern has a mainly horizontal orientation with additional secondary pattern variation at nearly a 90° angle to that (Figure 6c).

We used scanning electron microscopy (SEM) to better visualize regions of the tail surface that contained missing denticles or gaps in the skin surface (Figure 7). The tail surface of mature thresher sharks displayed numerous missing denticles (Figure 7a), and examination of these locations revealed that a number of the gaps contained denticles that appear to be replacement denticles emerging from the dermis below (Figure 7b–f). Images of the cut edge of the samples (Figure 7e) clearly show a denticle emerging into the gap above. These replacement denticles emerge crown first, and with all surface ridges fully formed.

3.2 | Embryo thresher shark tail denticle morphology

Thresher shark embryo tails are covered in a membrane that completely covers underlying dermal denticles (Figure 8). Peeling back the membrane (Figure 8a) reveals the underlying denticle surface, and histological analysis shows that denticles are overlain by this membrane and that a soft-tissue matrix extends in between adjacent denticles (Figure 8b). Comparative surface profilometry of the embryo tail with and without the membrane shows a nearly ten10-fold increase in surface roughness without the surface membrane (Figure 8c,d): surface height variation increases from 1–2 to 20 μm.

Denticles on embryo tails (Figures 8d and 9) are spaced more widely than in mature tails and we did not observe any missing denticles or gaps in the denticle pattern. The dispersed spacing of denticles with gaps causes thresher embryo tails to have, on average, larger roughness values than comparable locations on mature tails (Table 2).

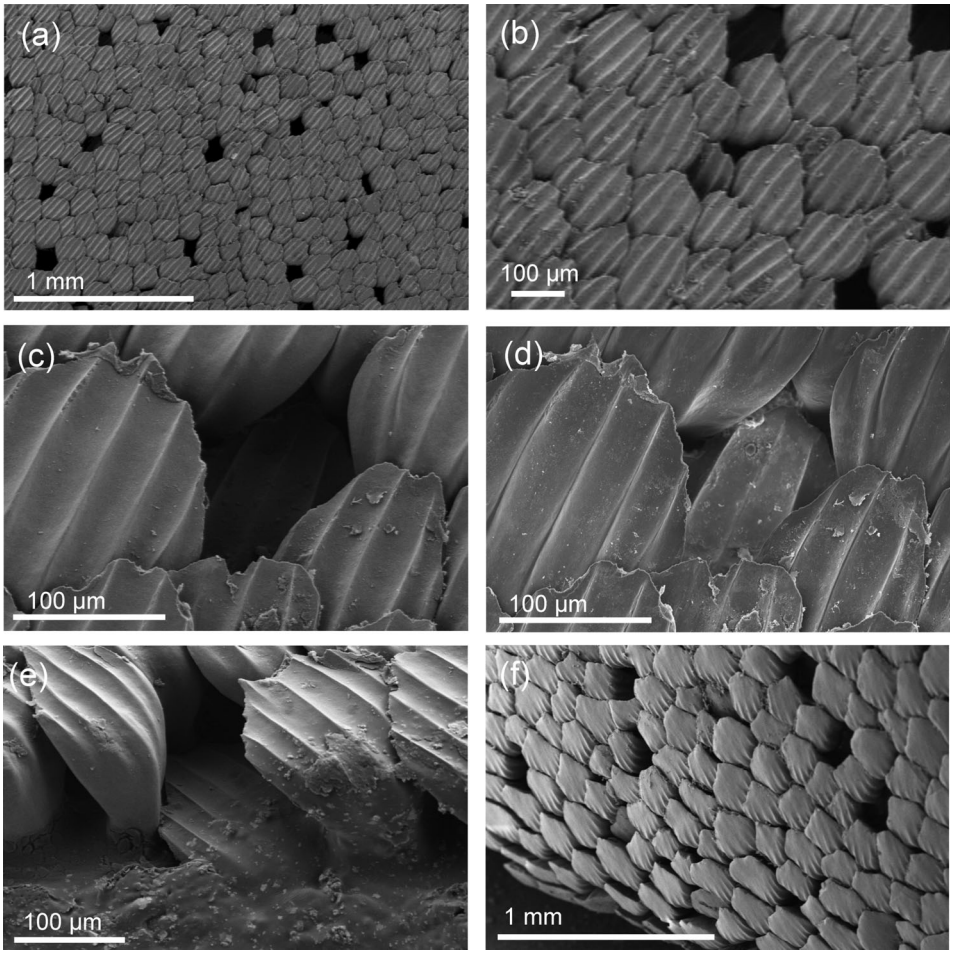

FIGURE 7 Scanning electron microscope images of denticles on a mature thresher shark tail. Panels (a) through (e) are taken from region #18 while panel (f) is taken from region #17 (see Figure 1b). Note the gaps in the denticle pattern shown in panels (a) and (b). These gaps are missing denticles. New denticles erupt from below to fill these gaps. Panels (c) and (d) are images of the exact same sample location taken with different electron beam angles to reveal the emerging subsurface denticle in the middle of the image. Panel (e) is imaged at the cut sample edge to show a sagittal view of a denticle emerging from the epidermis into the gap resulting from a missing denticle. Panel (f) shows the leading edge of the tail which also shows missing denticles and the reduced surface ridges present at this location

The leading edge of embryo tails is similar to mature tails in having flat and vertically oriented denticles with more spacing between them (Figure 9, compare 10, 50, and 90% span locations; Table 2). Denticles along the leading edge are larger than the middle surface and trailing edges. For example, at the 50% tail span location, denticles are 329, 136, and 132 μm long on average respectively (Table 2), which is similar to the mature tail pattern summarized in Table 1. Middle surface denticles on embryo tails have smaller widths than comparable denticles on mature tails and embryo denticles possess three ridges instead of five (Figure 9; Table 2).

3.3 | Variation among species in tail denticle morphology

Data from the mid-span and middle tail surface location (Figure 1b: sample #18) of 11 additional species illustrate the considerable diversity among the tail surfaces of mature sharks (Figure 10; Table 3). Tail denticles vary considerably in size with mako and thresher sharks possessing the smallest tail denticles (150–174 μm mean length), while other species such as leopard sharks have larger tail denticles nearly 600 μm long. Tail surface roughness (Sq) is lowest in mako and silky sharks (Table 3) which both possess tail surfaces with average roughness of 3.8 μm, while thresher, porbeagle, and blacktip sharks all possess tail roughnesses of 5–6 μm. Leopard sharks, blue sharks, and white sharks have rougher tail surfaces (10–20 μm). Basking sharks are unique among the diversity that we sampled in having both a rough surface (Sq = 25.1 μm) and small (216 μm) denticles (Table 3). This is due to the relatively wide spacing among denticles which produces increased topographic variation.

3.4 | Quantitative analyses of denticle variation

Variation in denticle characteristics among thresher shark tail locations is summarized in Figure 11. The length of leading edge denticles increased from the base to the distal tip of the tail, but middle surface and trailing edge denticles did not change dimensions. There was no significant change in denticle width along the length of the tail. Denticle ridge height decreased from the base (mean = 5 μm) to tail tip (3 μm) for the middle surface and trailing edges. However, the leading edge denticle ridges were prominent only at the tail base, and denticles beyond the 30% span had no significant ridges (Figure 11c). Ridge spacing also decreased along the tail span for middle and trailing tail locations. Denticle surface roughness was similar along the tail length for middle and trailing surfaces.

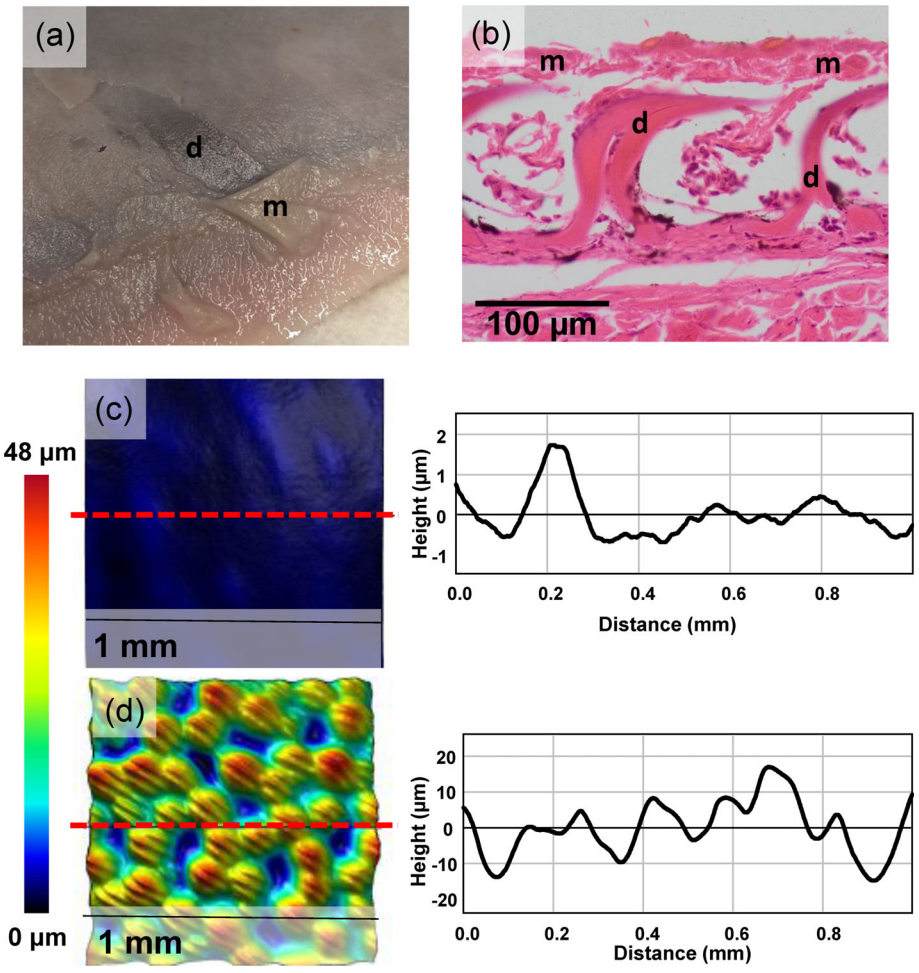

FIGURE 8 Surface structure of the tail in embryo thresher sharks. (a) Photograph of the embryo tail surface showing the membranous covering over the denticles (m) that has been peeled back in the image center to show the underlying denticle surface (d). Denticle histology is shown in panel (b). This sample is taken from a sagittal slice of the skin including the membrane (m, visible at the top of the image above the denticles, d). Anterior is to the left. Panel (c) corresponds to region (#18, Figure 1a) with the membranous covering intact. Panel (d) shows this same region after the membranous covering was removed. Color indicates height with blue corresponding to 0 μm and red to the maximum height of 48 μm; both (c) and (d) are shown at the same height scale). Anterior is left and images are 1 mm by 1 mm. To the right of each profilometry image is the surface elevation profile taken at the sample location indicated by the red dashed line. Graphs represent height relative to a mean height set to zero. Note the differing profile height axes: the presence of the membrane greatly reduces surface height variation. Quantitative values for embryo tail surface roughness are given in Table 2

However, the roughness of the leading edge more than doubled from base to tail tip.

Surface profilometry values collectively (Sq, Ssk, denticle length and width, aspect ratio, isotropy, texture direction 1, angle from flow axis, and ridge height) varied along the leading to trailing edge axis (MANOVA: Wilks trace F [16, 70] = 9.5, $p < .0001$). Separate ANOVAs on each of these variables showed a significant effect of surface roughness Sq (F [2, 42] = 20.7, $p < .0001$), texture direction 1 (F [2, 42] = 5.2, $p < .01$), angle from flow axis (F [2, 42] = 31.1, $p < .0001$), mean width (F [2, 42] = 54.6, $p < .0001$) and mean ridge height (F [2, 42] = 20.4, $p < .0001$), but not surface skew (Ssk) (F [2, 42] = 0.8, $p = .5$), isotropy (F [2, 42] = 0.9, $p = .4$), or denticle aspect ratio (F [2, 42] = 0.3, $p = .8$).

There was significant variation in surface profilometry data along the length of the tail (MANOVA: Wilks trace F [32, 123.29] = 1.7, $p = .02$). Separate ANOVAs on each of the eight variables showed that only mean ridge height varied along the length of the tail (F [4, 40] = 3.2, $p = .02$). There was no significant variation in roughness (Sq) (F [4, 40] = 0.9, $p = .5$), angle from flow axis (F [4, 40] = 0.9, p = 0.5), mean width (F [4, 40] = 0.3, $p = .9$), skew (Ssk) (F [4, 40] = 0.3, $p = .9$), isotropy (F [4, 40] = 1.7, $p = .2$), texture direction 1 (F [4, 40] = 1.7, $p = .2$), or denticle aspect ratio (F [4, 40] = 0.03, $p = 1.0$).

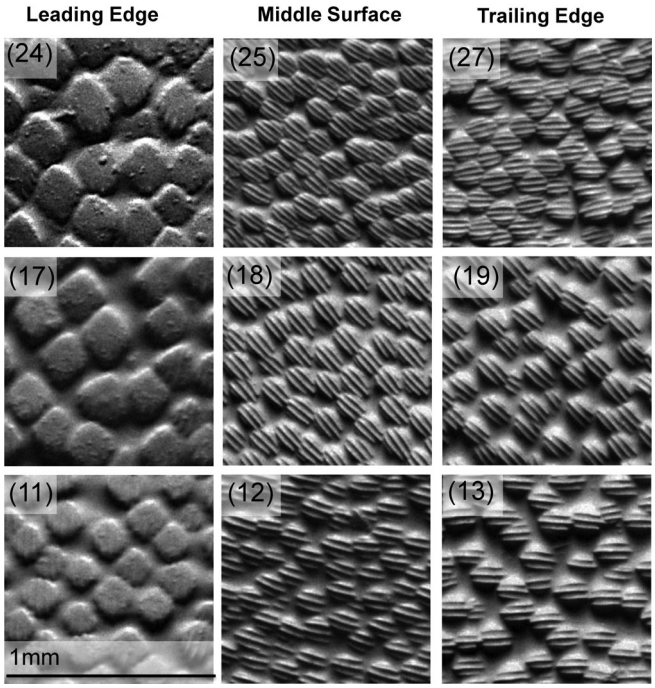

FIGURE 9 Images (obtained using surface profilometry, see Methods) of thresher shark embryo tails after removal of the membranous covering. Panels are labeled by the number corresponding to the locations in Figure 1a. Quantitative values for embryo tail surface roughness are given in Table 2. Note the lack of missing denticles compared to comparable images from mature tails shown in Figures 2 and 3. Scale bar refers to all panels. Anterior is to the left for middle and trailing edge samples; anterior is down for leading edge samples

Post-hoc tests revealed that the leading edge had significantly wider denticles and a higher surface roughness (Sq) than the middle surface (denticle width: $p < .0001$; Sq: $p < .0001$) or trailing edge (denticle width: $p < .0001$; Sq: $p < .001$). There was an increasing gradient of denticle ridge height across the tail, with the leading surface having lower ridges than the middle ($p < .001$) and trailing surface ($p < .0001$). Additionally, there was a decreasing gradient of ridge height along the length of the tail: the 10% span location had taller ridges than the 90% location ($p = .035$), but not significantly taller ridges than the 70% ($p = .06$) and 50% locations ($p = .078$).

Discriminant function (DF) analysis was performed to identify surface profilometry variables that best separate leading edge, middle surface and trailing edge groups of variables. DF1 accounts for 93.8% of the diversity among the tail locations (Figure 12a) while DF2 contributes the remaining 6.2% of variation. Along the span of the tail (Figure 12b), DF1 accounts for 56.6% of the variation while DF2 accounts for 28.8%.

Mature and embryo tail surface characteristics are significantly different from each other (Figure 12c; MANOVA: Wilks trace F [8, 71] = 15.7, $p < .0001$). Separate ANOVAs on each of eight variables showed embryo surfaces had a higher surface roughness (Sq, F [1, 78] = 64.7, $p < .0001$), lower skew (Ssk, F [1, 78] = 36.7, $p < .0001$), taller denticle ridges (F [1, 78] = 6.2, $p = .02$) and lower denticle aspect ratios (F [1, 78] = 12.8, $p < .001$). However, mature and embryo surfaces did not differ in their angle from the horizontal axis (F [1, 78] = 0.03, $p = .9$), mean width (F [1, 78] = 0.8, $p = .4$), isotropy (F [1, 78] = 1.5, $p = .2$), or texture direction 1 (F [1, 78] = 0.4, $p = .6$). These differences in surface characteristics allowed for 100% of the diversity among the groups to be accounted for by the first discriminant factor (Figure 12c).

4 | DISCUSSION

4.1 | Thresher shark tail denticles

Substantial variation in skin surface structure was found throughout the tails of both mature and embryo thresher sharks. Leading edge tail samples had higher roughness (Sq) values than other tail regions, in addition to having longer and wider denticles, and greatly reduced or absent ridges (Figure 11; Table 1). However, the middle surface and trailing edge regions were generally similar to each other in roughness, denticle length and width, and the presence of ridges. This pattern of tail surface variation was also seen in previous research on mako sharks, where the leading edge denticles were of larger size (Motta et al., 2012), and flat paver-like denticles that lack ridges are common on the leading edges of shark tails and fins (Ankhelyi et al., 2018), as well as other leading-edge surfaces like the rostrum. While the functional significance of the unique leading edge denticle shape remains unknown, flattened smooth denticles may provide both protection for the leading edge and reduce denticle damage due to impacts from small water-borne objects or organisms. We frequently observed damaged denticles where the flattened crown area was cracked or chipped on the tail surface, and the paver-like leading edge denticles

TABLE 2 Profilometry measurements for skin samples from embryo thresher sharks (*Alopias vulpinus*) with the covering membrane removed

Named region	Sample number	Sq (μm)	Ssk	Sku	Sz (μm)	Isotropy	Texture direction 1 (°)	Denticle length (μm)	Denticle width (μm)	Ridge height (μm)	Ridge spacing (μm)	Angle from flow axis (°)
Ventral tip	1	15.7	−0.1	2.4	85.3	81	−11	202	150	0	NA	9
V50% lead	2	10.5	−0.1	2.6	62.3	79	−42	299	234	0	NA	4
V50% mid	3	15.7	−0.2	2.5	86.7	81	8	199	157	7.6	41	14
V50% trail	4	14.8	0.2	2.4	78.6	80	−9	167	132	6.9	37	9
Central mid	7	10.1	0.6	2.9	55.9	72	0.1	193	148	9.5	46	15
Central trail	8	13.5	0.1	2.3	72.6	73	−8	203	144	8.4	41	12
D10% lead	11	12.2	−0.1	2.4	76.7	78	54	248	247	2.0	25	10
D10% mid	12	10.8	−0.1	2.6	61.9	85	14	186	128	7.1	38	15
D10% trail	13	15.3	0	2.3	89.6	86	0.2	191	136	8.6	37	3
D50% lead	17	15.0	−0.3	2.4	91.6	94	67	328	319	0	NA	2
D50% mid	18	10.0	−0.3	2.8	61.3	83	50	183	136	6.3	37	39
D50% trail	19	13.9	−0.3	2.3	68.3	80	45	184	132	6.3	37	35
D lobe	23	9.8	−0.1	2.3	54.2	83	27	169	136	3.4	34	26
D90% lead	24	11.9	−0.4	2.4	65.6	78	44	342	282	0	NA	6
D90% mid	25	10.8	−0.6	3.4	72.3	87	34	171	148	3.7	35	41
Dorsal tip	27	10.3	−0.3	3.0	60.9	69	17	290	158	2.3	16	1

Note: Variation among locations is shown in Figure 11. Values shown are means (N = 2 individuals, for metrics of surface roughness; N = 3 denticles from each of the two embryo individuals for the length, width, height and spacing measurements). Sample numbers (locations along the tail) are provided in Figure 1. Detailed variable descriptions are provided in the Methods section. NA indicates no ridge spacing when denticle ridges have zero height (i.e., ridges are absent).

Abbreviations: D, dorsal; lead, leading edge; lobe, subterminal lobe; mid, middle/lateral portion of the body; Sku, kurtosis; Sq, roughness; Ssk, skew; Sz, maximum feature height; tip, tip of the caudal fin; trail, trailing edge; V, ventral.

may be less susceptible to such damage. Tail surface denticles have ridges generally aligned along the direction of presumed flow, although flow along a deforming tail like that of a thresher shark is likely to be complex and multidirectional. Leading edge denticles encounter free-stream flow that is changing direction as the tail beats back and forth (Ferry & Lauder, 1996; Wilga & Lauder, 2004) which also may explain their lack of ridges.

Overall tail surface roughness is a function of both the surfaces of individual denticles and spaces among denticles which can greatly increase surface roughness. Smaller denticles can be correlated with lower Sq values (Table 3) as also shown for smooth dogfish by Ankhelyi et al. (2018). But in thresher sharks, larger Sq values also reflect increases in the number of missing denticles and the space between denticles. Leading edge Sq values are larger because denticles are larger and there are more spaces between adjacent denticles which leads to greater surface topographic variation. Embryo tails show the strong effect that space between denticles can have on roughness. Even though embryo tails have smaller denticles than mature sharks (Figure 8d), embryo tails have larger roughness values (Tables 2 and 3) due to the increased spacing among embryo denticles which causes increased surface topographic variation in height.

The number of gaps in the denticle surface on mature thresher shark tails was noteworthy, and we frequently observed what appear to be missing denticles at all locations along the tail in the surface profilometry images (Figures 2 and 3). The tail surface has similar overall numbers of missing denticles from the base toward the tip, but the trailing edge all along the length of the tail has greater numbers of missing denticles than the middle or leading edge regions. Imaging with scanning electron microscopy (SEM) clearly revealed gaps in the tail surface that are consistent with missing individual denticles (Figure 7a), and close examination of these gaps showed apparent replacement denticles emerging into the space between denticles (Figure 7b–d). Denticles that emerge into the gaps have fully-formed crowns that are tilted up, and replacement denticles must then rotate toward the skin surface to fill in the gap. We were able to locate a replacement denticle emerging through the dermis and epidermis into a gap between adjacent denticles by imaging along the edge of cut SEM samples (Figure 7e). We are not aware of previous reports of surface gaps with evidence of denticle replacement in shark skin, as published images of shark skin denticle surfaces typically show a small number of denticles with none missing. But we expect that missing denticles are a common feature of shark surfaces as we observed these gaps in all species analyzed for Table 3. Shark denticles found in sediments have been used to reconstruct community structure (Dillon, Norris, & O'Dea, 2017) and our results suggest that these denticles may include denticles lost from the skin surface as part of normal denticle replacement. Thresher shark tails, with the large amplitude whip-like movements that occur during feeding and the

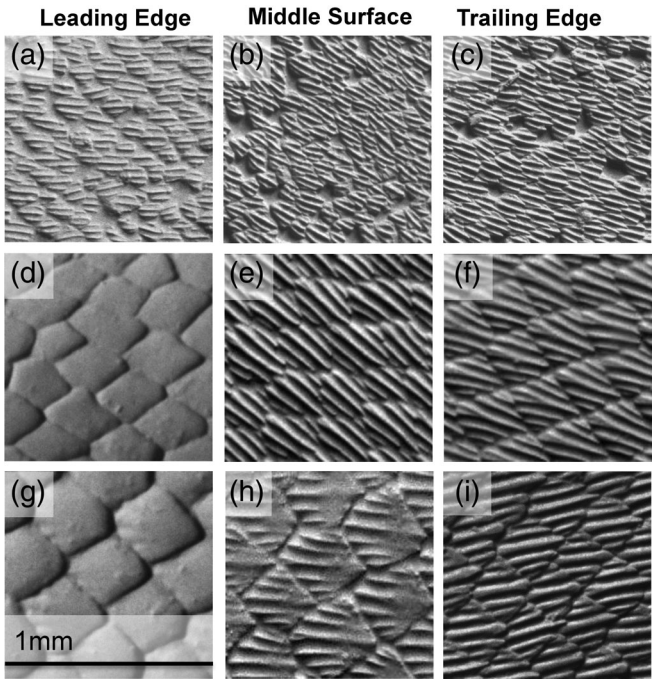

FIGURE 10 Comparative denticle surface profilometry images (see Methods) from the tails of three shark species for comparison to thresher shark tail data. (a, b, c): Shortfin mako shark, *Isurus oxyrinchus*. (d, e, f): bonnethead shark, *Sphyrna tiburo*. (g, h, i): blacktip shark, *Carcharhinus limbatus*. Each of the three rows contains one sample from the leading edge, middle surface and trailing edge respectively at the 50% span location along the tail corresponding to approximately thresher shark sample locations 17, 18, and 19 in Figure 1b. Measurements of surface characteristics in these and other comparative species are given in Table 3. Scale bar refers to all panels. Anterior is to the left for middle and trailing edge samples; anterior is down for leading edge samples

extreme undulatory tail motion during steady swimming, might be expected to exhibit increased numbers of missing denticles relative to benthic species and species that use their tails for locomotion only. Analyses of differences in denticle replacement patterns around the body and among species that differ in ecology is a promising area for future investigation.

Other noteworthy gradients in tail denticle structure include changes in denticle aspect ratio along the span. Leading edge denticles become increasingly elongate and narrow toward the tail tip, while denticles increase in width along the middle and trailing edge surfaces along the tail span to assume a square-like shape with aspect ratios approaching 1.0 (Figure 11h). Elongation of leading edge denticles may be due in part to the narrowing of the leading edge of the distal tail in order to establish a continuously tiled surface even around the relatively high-curvature leading edge near the tail tip.

Ankhelyi et al. (2018) showed that the skew (Ssk) values measured from surface profilometry on smooth dogfish skin are largely *negative*, indicating the presence of relatively more valleys or pits than peak-like surface features. This finding was of interest because previous research on the skin surface of teleost fishes had shown that low *positive* skew values dominate (Wainwright et al., 2017; Wainwright & Lauder, 2016). Our results from thresher shark tails confirm the dominance of negative Ssk values for shark skin, and that the tail surface of most other shark species (Table 3) is also characterized by negative skew values. Gaps among denticles will certainly contribute to negative skew, and the greater spacing of embryo tail denticles also produces negative Ssk values. Shark skin skew values also contrast with the skin surface of cetaceans (Wainwright et al., 2019) which has positive skew values.

Cetacean skin also has kurtosis (Sku) values up to 28 for bottlenose dolphin (Wainwright et al., 2019), while kurtosis values that we measured for thresher shark tails ranged from 3.2 to 13.8 for mature tails and from 2.3 to 3.0 for embryos. Thresher embryo tails thus differ from both mature individuals and cetacean skin in having relatively less variation in height which could be due to both relatively widely-spaced denticles as well as denticles that have not fully erupted from the skin surface to their full mature height.

Maximum height (Sz, the maximum height as a distance from the lowest surface point, Tables 1–3) is an aspect of skin surface structure that may be particularly relevant to swimming hydrodynamics, as this value indicates the extent to which surface structures could project into fluid flowing past the tail, depending on boundary layer thickness. For mature tails, Sz ranged from 35.2 to 112.3 μm, while embryo Sz values ranged from 54.15 to 91.6 μm. The nature of the boundary layer on the tail of thresher sharks during swimming is not known, but the increase in leading edge Sz values from the base of the tail toward the tip indicates a correlation between roughness at this location on the tail and the amplitude of oscillatory movement based on field video data of thresher shark locomotion.

Isotropy values of mature thresher shark tails were all above 30, indicating that the surface texture is effectively isotropic overall, despite having surface ridges on individual denticle surface elements. The longitudinal ridges are clearly directional, but the ridges are small in terms of height and their directional signal is probably obscured by much larger height differences among denticles.

Analysis of two tails from thresher shark embryos revealed that the tails are covered with a soft-tissue membrane (up to 20 μm thick) that provides a much smoother surface than the mature shark's denticle-covered tail surface (Figure 8). Embryo tails also have higher surface ridges on denticle crowns on average than mature thresher tails. We hypothesize that thresher shark embryos possess membranes that cover the rough surfaces of developing denticles to protect maternal tissues from abrasive damage when embryos move. Intrauterine locomotor movement by embryos is well documented in sharks (Tomita, Murakumo, Ueda, Ashida, & Furuyama, 2019) and the greatly enlarged tail of thresher embryos may pose a particular maternal hazard unless the tail surface is protected by a smooth covering. Many sharks give birth to live young through either viviparity or ovoviviparity, and soft membranes that cover embryo skin may be a widespread trait to protect the mother and siblings from abrasion. Presumably this membrane is shed after birth when free-swimming begins. The occurrence of a covering surface membrane in thresher shark embryo tails has, to our knowledge, not been previously documented, and verifying the presence of such a protective structure in the embryos of other species would be of interest.

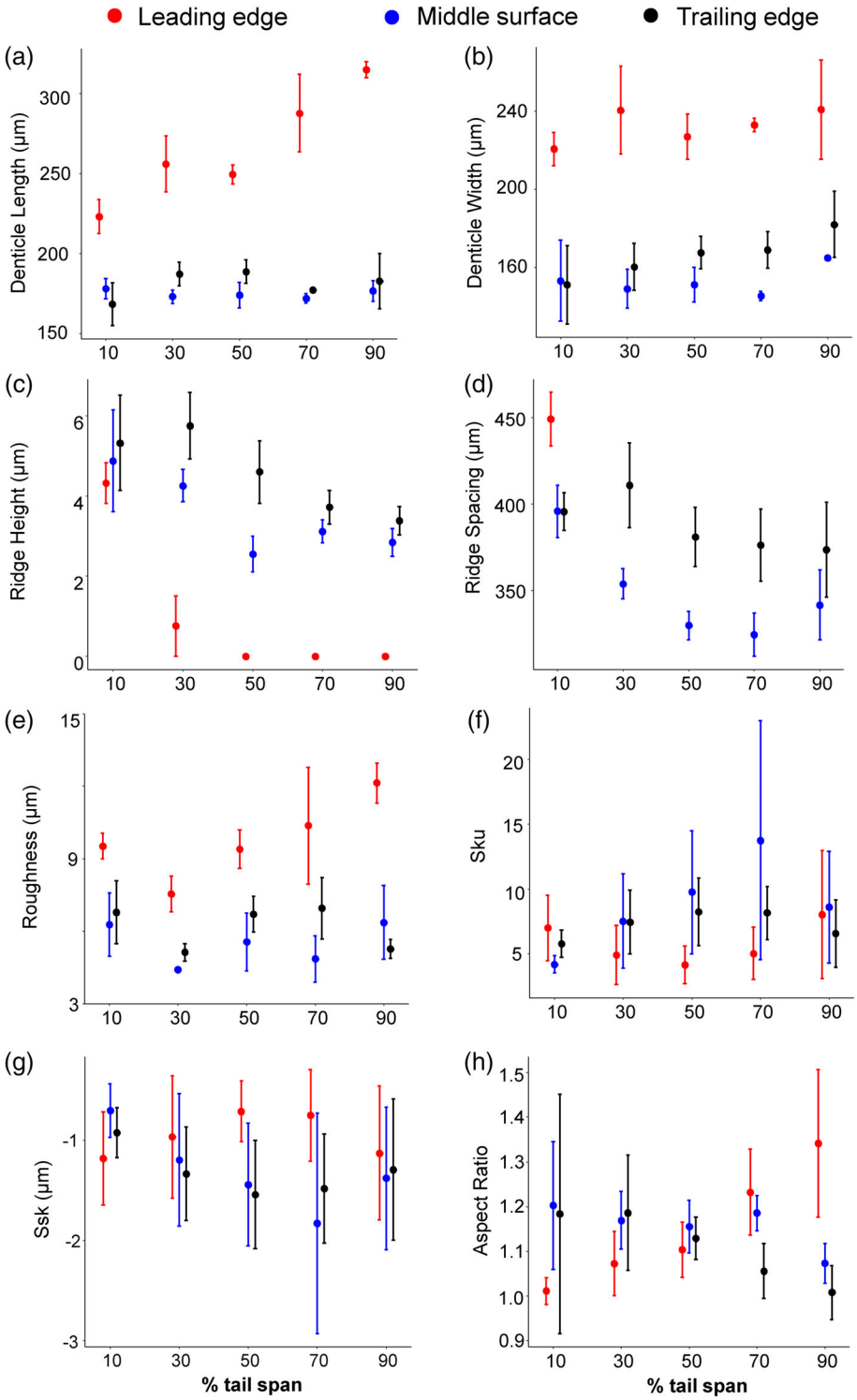

FIGURE 11 Summary of variables measured from surface profilometry images comparing measurements of denticles from different span locations and the leading edge, middle surface, and trailing edge on the tails of mature thresher sharks. The x-axis of all graphs is the percentage distance along the mature tail, and *N* = 3 tails were studied. See Figure 1b for the specific sample regions that are associated with these general areas. All plots show the mean ± SD. (a) denticle length (µm), (b) denticle width (µm), (c) ridge height (µm), (d) ridge spacing (µm), (e) roughness (µm), (f) kurtosis (Sku), (g) skew (Ssk), (h) average denticle aspect ratio. Details on how each variable was measured are given in the methods

4.2 | Denticle roughness gradients and hypothesized function

The roughness of a surface in contact with a moving fluid can have substantial effects on the character of flow near that surface and on the nature of the shear stress in the boundary layer, which determines one component of drag (Schetz, 1993; Smits, 2000; Vogel, 1994). Effects of surface roughness are extremely complex, and depend on the scale of the roughness, orientation of surface elements, fluid velocity, Reynolds number, and the movement of

TABLE 3 Denticle surface structure from eleven shark species compared to the common thresher in table row one

Species	Sq (μm)	Ssk	Sku	Sz (μm)	Denticle length (μm)	Denticle width (μm)
Common thresher (*Alopias vulpinus*)	5.6	−1.4	9.8	62.9	174	151
Shortfin mako (*Isurus oxyrinchus*)	3.8	−0.2	3.7	34.6	150	097
Silky shark (*Carcharhinus falciformis*)	3.8	−0.3	3.45	32.3	222	153
Bonnethead (*Sphyrna tiburo*)	5.0	0.1	3.0	35.6	303	242
Porbeagle (*Lamna nasus*)	5.5	−0.3	3.1	37.3	252	252
Blacktip (*Carcharhinus limbatus*)	5.7	−0.5	3.5	51.5	471	456
Leopard shark (*Triakis semifasciata*)[a]	10.7	−0.3	3.0	69.6	580	442
Blue shark (*Prionace glauca*)	11.2	−0.1	2.4	56.1	321	233
Spiny dogfish (*Squalus acanthias*)[a]	16.7	−0.2	2.9	137.0	345	299
White shark (*Carcharodon carcharias*)	17.3	−0.5	3.8	143.7	370	263
Basking shark (*Cetorhinus maximus*)	25.1	0.7	3.0	129.0	216	188
Smooth dogfish (*Mustelus canis*)[a]	17.3	−0.7	3.8	143.7	370	263

Note: All samples are from the mid-tail location at 50% span, approximately sample location #18 (Figure 1b), from one individual in each species. $N = 3$ denticles from each individual for the denticle length and width measurements; table entries are means. Detailed variable descriptions are provided in the Methods section.

Abbreviations: Sku, Kurtosis; Sq, roughness; Ssk, skew; Sz, maximum feature height.

[a]From Ankhelyi et al. (2018).

the surface (Raayai-Ardakani & McKinley, 2019). This latter feature, how any particular surface moves in flow, is particularly difficult to correlate with specific effects on the boundary layer: analyses of moving biological surfaces and how motion affects near-surface flow dynamics have proven to be challenging to perform (Anderson, McGillis, & Grosenbaugh, 2001; Eloy, 2013; Lauder et al., 2016; Taneda & Tomonari, 1974; Yanase & Saarenrinne, 2015). Although large-scale surface roughness will generally increase drag, some particular roughness patterns (e.g., riblets, shark denticles, dimples) can have positive effects on the boundary layer (and decrease drag) by "tripping" the boundary layer from laminar to turbulent, delaying flow separation (Lang et al., 2014).

Due to the dramatic undulatory gradient along the thresher shark tail that is clearly evident in videos of thresher sharks swimming and feeding (Aalbers et al., 2010; Oliver et al., 2013), we expected that tail surface roughness should increase toward the tail tip if there is a correlation between the amplitude of undulatory motion and surface roughness. Rougher surfaces that experience higher amplitude motion may reduce drag by inducing turbulent flow. Our data on tail surface roughness for the middle and trailing edge regions (Figure 11; Table 1) do not support this hypothesis, and thresher shark tail surface roughness remains largely constant among these regions, averaging 5.6 μm along the tail. However, water flow around the tail leading edge could also be impacted by roughness of this surface, and indeed we observed that leading edge roughness increases from the tail base toward the tip, increasing from 7.5 μm at the 30% span location to 12.1 μm at the 90% leading edge span position, supporting the initial hypothesis for the tail leading edge (Figure 11e). With quantitative knowledge of the extent and magnitude of tail surface roughness variation in hand, laboratory experiments under controlled conditions could be performed with manufactured surfaces using these known roughness values to analyze the effect of different shark-tail-like roughness patterns on near-surface flows.

4.3 | Comparison of skin surface structure among species

Measurements of shark tail characteristics using surface profilometry at the mid-tail location (Table 3) show that there is substantial variation in three-dimensional skin surface structure among different shark species. Denticles of shortfin mako, a high-speed oceanic species, are considerably smaller than in other species (0.15 μm in length and 0.10 μm in width), and makos had the smallest Sq value of 3.8 μm, indicating a very smooth skin surface (only the silky shark, a pelagic and highly migratory species, is as smooth). Thresher shark skin roughness is generally comparable to that of silky, mako, bonnethead, porbeagle, and blacktip sharks (Table 3) all of which are active swimmers. The diversity of tail surface roughness appears to generally correlate with routine swimming speeds with more active sharks possessing smaller denticles, but it is noteworthy that white sharks (also active swimmers) have skin roughness approximately three times higher than that of thresher, mako, and porbeagle. Ranking different shark species by both routine swimming speed and maximal burst speed is subject to considerable error due to the lack of quantitative data on the diversity and frequency of different locomotor behaviors. Tail surface metrology shows that sharks as divergent in ecology and locomotor style as white sharks (which actively feed on larger prey and can undertake long-distance migrations) and spiny dogfish (a more benthic species maturing at a smaller body size; Camhi, Pikitch, & Babcock, 2008; Castro, 2011) have similar tail surface roughness

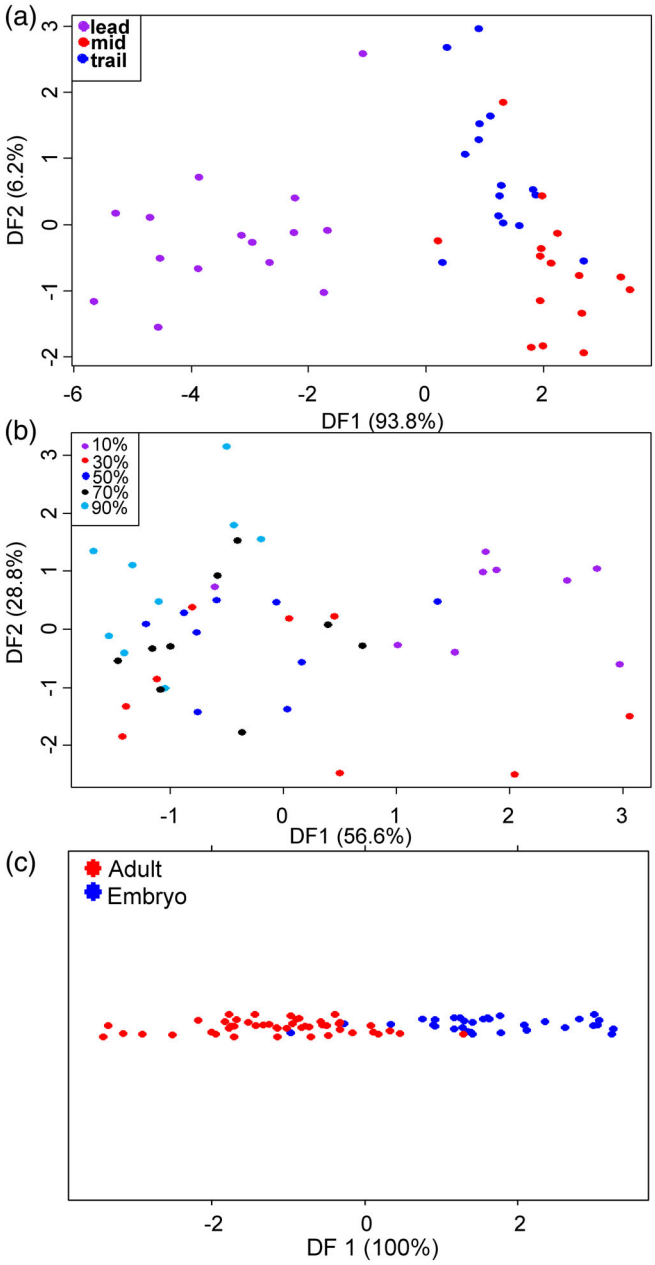

FIGURE 12 Discriminant function analysis (DFA) of denticle variables to summarize multivariate patterns in denticle data from thresher shark tails. Percentages in parentheses on axis labels are the percentage of the diversity among groups. Plots (a) and (b) show DF2 versus DF1 for mature tails only. Panel (c) shows only DF1 because there are just two categories (mature and embryo). Point colors indicate different tail regions (a), position of denticles along the tail span (b), or mature versus embryo denticles (c). (a) DFA on surface profilometry data using eight variables categorized by leading edge, middle surface, and trailing edge. (b) Discriminant function analysis on surface profilometry data using eight different variables categorized by tail span percentage. (c) Discriminant function analysis on surface profilometry data using eight different variables categorized by mature (N = 3) and embryo (N = 2) tails. Denticle measurements for embryo tails are after removal of the covering membrane. Points are jittered to better visualize individual measurements. Statistical analysis (see text) demonstrates a significant difference among body regions in denticle morphology and between mature and embryo denticles

values of 17 μm, suggesting that surface characteristics can be similar even in sharks with different locomotor lifestyles. Thresher shark tails have the most negative skew (Ssk) values, most likely reflecting the larger number of missing denticles and had the largest kurtosis (Sku) values in comparison to other species, indicating that higher peaks and lower valleys are present than in other species, probably also the result of the relatively large number of missing denticles on thresher tails.

4.4 | Future directions

The comparative study of three-dimensional surface structure in biological surfaces is still in its infancy (Wainwright et al., 2017), and the acquisition of additional data in the context of fluid flow over shark-like textured surfaces would be valuable in two specific contexts: a comparative approach and experimental research. Comparative test cases such as the thresher shark tail take advantage of a specific biological novelty with extreme kinematics to investigate the correlation between motion and skin surface structure. Other such cases where the shark skin surface undergoes motions that might be associated with particular denticle textures will allow a better understanding of correlations between denticle surfaces and fluid flow patterns. For example, Frumkin and Shimada (2020) compared several denticle metrics in different thresher species to other lamniform sharks to determine if it was possible to correlate two-dimensional denticle characteristics with hypothesized tail motion and interspecific locomotor activity patterns. They were able to establish several general correlations between denticle morphometric patterns and behavior, and as more information becomes available on free-swimming shark locomotor behaviors this approach may yield more precise correlations.

Future experimental studies using 3D-printed denticle patterns and different imposed flow regimes in the laboratory will allow causal relationships between denticle surfaces and water flow patterns to be uncovered. Quantitative analysis of near-surface flow patterns and measurement of boundary layer flows over different biomimetic roughness patterns is best conducted under controlled laboratory conditions. And by combining comparative and experimental investigations, we can better understand the relationship between the remarkable diversity of shark skin surfaces and fluid flow patterns that they experience.

ACKNOWLEDGMENTS

Many thanks to Kady Lyons and Laura Martinez-Steele for obtaining one mature thresher shark tail and two thresher embryo tails, and to Prof. Chris Lowe for his assistance in specimen collection. We thank Cathy MacGillivray in Harvard's Stem Cell and Regenerative Biology's Histology-Immunochemistry Core for assistance with preparation of the histology sections and Jacob Suissa for initial assistance in obtaining images of replacement denticles. Dr James Weaver of the Wyss Institute at Harvard acquired the GelSight system which has been crucial for gathering information on biological imaging. Thanks

also to Molly Gabler Smith for comments on the manuscript and to members of the Lauder Laboratory for assistance with this research. This paper is dedicated to the memory of Linda Popp (1961-2019). This study was funded by a Harvard College Research Program grant and a Museum of Comparative Zoology Grant-In-Aid of Undergraduate Research to MP, NSF GRF DGE-1144152 to DKW, ONR MURI Grant No. N000141410533 monitored by Bob Brizzolara to GVL, Office of Naval Research grant N00014-09-1-0352 monitored by Dr Thomas McKenna to GVL, and NSF IOS-1354593 and NOAA NA16NMF4270231 to DB. Any opinions, findings, and conclusions or recommendations expressed in this material are those of the author(s) and do not necessarily reflect the views of the National Science Foundation or NOAA.

CONFLICT OF INTEREST

All authors declare no conflicts of interest.

AUTHOR CONTRIBUTIONS

Dylan K. Wainwright and George V. Lauder designed the study. Connor F. White and Diego Bernal collected specimens and contributed to data presentation and analysis. Meagan Popp conducted the majority of the imaging data acquisition, measured the denticles, and prepared figures. Dylan K. Wainwright designed the measurement protocol and developed the statistical analysis approach. Meagan Popp wrote the first draft of the manuscript, and all authors collaborated on interpreting the data, in revising the manuscript and figures, and preparation of the final manuscript.

DATA AVAILABILITY STATEMENT

Data available upon request to the authors.

ORCID

Meagan Popp https://orcid.org/0000-0003-0201-6420
Connor F. White https://orcid.org/0000-0001-8260-290X
Diego Bernal https://orcid.org/0000-0002-4192-9559
Dylan K. Wainwright https://orcid.org/0000-0003-4964-5048
George V. Lauder https://orcid.org/0000-0003-0731-286X

REFERENCES

Aalbers, S., Bernal, D., & Sepulveda, C. (2010). The functional role of the caudal fin in the feeding ecology of the common thresher shark *Alopias vulpinus*. *Journal of Fish Biology*, *76*, 1863–1868.

Anderson, E. J., McGillis, W., & Grosenbaugh, M. A. (2001). The boundary layer of swimming fish. *Journal of Experimental Biology*, *204*, 81–102.

Ankhelyi, M., Wainwright, D. K., & Lauder, G. V. (2018). Diversity of dermal denticle structure in sharks: Skin surface roughness and three-dimensional morphology. *Journal of Morphology*, *279*, 1132–1154.

Baeckens, S., Wainwright, D. K., Weaver, J. C., Irschick, D. J., & Losos, J. B. (2019). Ontogenetic scaling patterns of lizard skin surface structure as revealed by gel-based stereo-profilometry. *Journal of Anatomy*, *235*, 346–356.

Bechert, D. W., Hoppe, G., & Reif, W.-E. (1985). On the drag reduction of the shark skin. *AIAA Journal*, *85-0546*(1985), 1–18.

Camhi, M. D., Pikitch, E. K., & Babcock, E. A. (2008). *Sharks of the open ocean: Biology, fisheries and conservation*. New York, NY: John Wiley & Sons.

Castro, J. I. (2011). *The sharks of North America*. Oxford: Oxford University Press.

Díez, G., Soto, M., & Blanco, J. M. (2015). Biological characterization of the skin of shortfin mako shark *Isurus oxyrinchus* and preliminary study of the hydrodynamic behaviour through computational fluid dynamics. *Journal of Fish Biology*, *87*, 123–137.

Dillon, E. M., Norris, R. D., & O'Dea, A. (2017). Dermal denticles as a tool to reconstruct shark communities. *Marine Ecology Progress Series*, *566*, 117–134.

Domel, A. G., Domel, G., Weaver, J., Saadat, M., Bertoldi, K., & Lauder, G. V. (2018). Hydrodynamic properties of biomimetic shark skin: Effect of denticle size and swimming speed. *Bioinspiration & Biomimetics*, *13*, 056014.

Domel, A. G., Saadat, M., Weaver, J., Haj-Hariri, H., Bertoldi, K., & Lauder, G. V. (2018). Shark denticle-inspired designs for improved aerodynamics. *Journal of the Royal Society Interface*, *15*, 20170828.

Dotson, C. L. (2015). *Fundamentals of dimensional metrology* (6th ed.). Boston, Mass: Centage Learning.

Eloy, C. (2013). On the best design for undulatory swimming. *Journal of Fluid Mechanics*, *717*, 48–89.

Fernandez-Waid, P., Diez, G., Bidaguren, I., Izagirre, U., Blanco, J. M., & Soto, M. (2019). Morphological characterization and hydrodynamic behavior of shortfin mako shark (*Isurus oxyrinchus*) dorsal fin denticles. *Journal of Bionic Engineering*, *16*, 730–741.

Ferry, L. A., & Lauder, G. V. (1996). Heterocercal tail function in leopard sharks: A three-dimensional kinematic analysis of two models. *Journal of Experimental Biology*, *199*, 2253–2268.

Frumkin, J. A., & Shimada, K. (2020). Integument-based inferences on the swimming ability and prey hunting strategy of the bigeye thresher shark, *Alopias superciliosus* (Lamniformes: Alopiidae). *Zoomorphology*, *139*, 213–229.

Johnson M. K. & Adelson E. H. *Retrographic sensing for the measurement of surface texture and shape*. 2009 IEEE Conference on Computer Vision and Pattern Recognition, Miami, FL, 2009. pp. 1070–1077.

Lang, A. W., Bradshaw, M. T., Smith, J. A., Wheelus, J. N., Motta, P. J., Habegger, M. L., & Hueter, R. E. (2014). Movable shark scales act as a passive dynamic micro-roughness to control flow separation. *Bioinspiration & Biomimetics*, *9*, 036017.

Lang, A. W., Motta, P., Hidalgo, P., & Westcott, M. (2008). Bristled shark skin: A microgeometry for boundary layer control? *Bioinspiration & Biomimetics*, *3*, 046005.

Lauder, G. V., & DiSanto, V. (2015). Swimming mechanics and energetics of elasmobranch fishes. In R. E. Shadwick, A. P. Farrell, & C. J. Brauner (Eds.), *Fish physiology, physiology of elasmobranch fishes: Structure and interaction with environment* (Vol. 34A, pp. 219–253). New York, NY: Academic Press.

Lauder, G. V., Wainwright, D. K., Domel, A. G., Weaver, J., Wen, L., & Bertoldi, K. (2016). Structure, biomimetics, and fluid dynamics of fish skin surfaces. *Physical Review Fluids*, *1*, 060502.

Motta, P., Habegger, M. L., Lang, A., Hueter, R., & Davis, J. (2012). Scale morphology and flexibility in the shortfin mako *Isurus oxyrinchus* and the blacktip shark *Carcharhinus limbatus*. *Journal of Morphology*, *273*, 1096–1110.

Oeffner, J., & Lauder, G. V. (2012). The hydrodynamic function of shark skin and two biomimetic applications. *Journal of Experimental Biology*, *215*, 785–795.

Oliver, S. P., Turner, J. R., Gann, K., Silvosa, M., & D'Urban, J. T. (2013). Thresher sharks use tail-slaps as a hunting strategy. *PLoS One*, *8*, e67380.

Preti A., Smith S. E. & Ramon D. (2001). *Feeding habits of the common thresher shark (Alopias vulpinus) sampled from the California-based drift gill net fishery, 1998-1999*. California Cooperative Oceanic Fisheries Investigations Report, pp. 145–152.

Raayai-Ardakani, S., & McKinley, G. H. (2019). Geometric optimization of riblet-textured surfaces for drag reduction in laminar boundary layer flows. *Physics of Fluids*, *31*, 053601.

Raghavendra, N., & Krishnamurthy, L. (2013). *Engineering metrology and measurements*. Oxford, U.K.: Oxford University Press.

Rangel, B. D. S., Amorim, A. F., Kfoury, J. R., Jr., & Rici, R. E. (2019). Microstructural morphology of dermal and oral denticles of the sharpnose sevengill shark *Heptranchias perlo* (Elasmobranchii: Hexanchidae), a deep-water species. *Microscopy Research and Technique*, *82*, 1243–1248.

Raschi, W., & Tabit, C. (1992). Functional aspects of placoid scales: A review and update. *Australian Journal of Marine and Freshwater Research*, *43*, 123–147.

Reif, W. (1982). Morphogenesis and function of the squamation in sharks. *Neues Jahrbuch für Geologie Und Paläontologie, Abhandlungen*, *164*, 172–183.

Reif, W. E. (1985b). Functions of scales and photophores in mesoplagic luminescent sharks. *Acta Zoologica*, *66*, 111–118.

Reif, W.-E. (1985a). Morphology and hydrodynamic effects of the scales of fast swimming sharks. *Fortschritte der Zoologie*, *30*, 483–485.

Schetz, J. A. (1993). *Boundary layer analysis*. Upper Saddle River, New Jersey: Prentice Hall.

Schlichting, H. (1979). *Boundary-layer theory*. New York, NY: McGraw Hill.

Smith, S. E., Rasmussen, R. C., Ramon, D. A., & Cailliet, G. M. (2008). The biology and ecology of thresher sharks (Alopiidae). In M. D. Camhi, E. K. Pikitch, & E. A. Babcock (Eds.), *Sharks of the open ocean: Biology, fisheries and conservation* (pp. 60–68). New York, NY: John Wiley & Sons.

Smits, A. J. (2000). *A physical Introduction to fluid mechanics*. New York, NY: John Wiley & Sons.

Southall, E. J., & Sims, D. (2003). Shark skin: Function in feeding. *Proceedings of the Royal Society of London B: Biological Sciences*, *270*, S47–S49.

Taneda, S., & Tomonari, Y. (1974). An experiment on the flow around a waving plate. *Journal of the Physical Society of Japan*, *36*, 1683–1689.

Tomita, T., Murakumo, K., Ueda, K., Ashida, H., & Furuyama, R. (2019). Locomotion is not a privilege after birth: Ultrasound images of viviparous shark embryos swimming from one uterus to the other. *Ethology*, *125*, 122–126.

Vogel, S. (1994). *Life in moving fluids. The physical biology of flow* (2nd ed.). Princeton: Princeton University Press.

Wainwright, D. K., Fish, F. E., Ingersoll, S., Williams, T. M., St Leger, J., Smits, A. J., & Lauder, G. V. (2019). How smooth is a dolphin? The ridged skin of odontocetes. *Biology Letters*, *15*, 20190103.

Wainwright, D. K., & Lauder, G. V. (2016). Three-dimensional analysis of scale morphology in bluegill sunfish, *Lepomis macrochirus*. *Zoology*, *119*, 182–195.

Wainwright, D. K., Lauder, G. V., & Weaver, J. C. (2017). Imaging biological surface topography *in situ* and *in vivo*. *Methods in Ecology and Evolution*, *8*, 1626–1638.

Wen, L., Weaver, J. C., & Lauder, G. V. (2014). Biomimetic shark skin: Design, fabrication, and hydrodynamic function. *Journal of Experimental Biology*, *217*, 1656–1666.

Wen, L., Weaver, J. C., Thornycroft, P. J. M., & Lauder, G. V. (2015). Hydrodynamic function of biomimetic shark skin: Effect of denticle pattern and spacing. *Bioinspiration & Biomimetics*, *10*, 1–13.

Westfall, P. H. (2014). Kurtosis as peakedness, 1905–2014. RIP. *The American Statistician*, *68*, 191–195.

Wilga, C. D., & Lauder, G. V. (2004). Hydrodynamic function of the shark's tail. *Nature*, *430*, 850.

Yanase, K., & Saarenrinne, P. (2015). Unsteady turbulent boundary layers in swimming rainbow trout. *Journal of Experimental Biology*, *218*, 1373–1385.

SUPPORTING INFORMATION

Additional supporting information may be found online in the Supporting Information section at the end of this article.

How to cite this article: Popp M, White CF, Bernal D, Wainwright DK, Lauder GV. The denticle surface of thresher shark tails: Three-dimensional structure and comparison to other pelagic species. *Journal of Morphology*. 2020;1–18. https://doi.org/10.1002/jmor.21222

Supplemental Material

Comparative biomimetic surface roughness

Shark skin has been of interest to researchers aiming to manufacture biomimetic surfaces for use in engineered platforms with the aim of taking advantage of hydrodynamic properties of shark skin (Bechert et al., 2000; Domel et al., 2018a; Domel et al., 2018b; Jung and Bhushan, 2010; Wen et al., 2014). Current additive manufacturing technology does not accurately reproduce shark skin structures at the size scale necessary to replicate shark denticles in three dimensions, and current three-dimensional prints result in denticle lengths on the order of 1.0 mm, albeit with considerably smaller surface ridges and other surface ornamentation (Domel et al., 2018a). Biomimetic 3d-printed shark skin at the smallest scale has surface roughness (Sq) of 150 μm, which is approximately ten times that of average shark tail skin (Domel et al., 2018a). And although shark skin has provided inspiration for competition swim suit design (Krieger, 2004) and other biomimetic surfaces (Dean and Bhushan, 2010; Lang et al., 2011), there is little quantitative comparative data on three-dimensional surface roughness to allow assessment of the extent to which manufactured surfaces compare to biological shark skin.

To provide data on different surfaces for comparison to thresher shark tail roughness, we used surface profilometry to quantify surface characteristics of six competition-quality swimsuits in addition to samples of other surfaces of interest with respect to texture and fluid flow (Supplemental Table S1). Competitive swim suit roughness ranged from 3.6 μm (similar to the mako shark tail surface) to 26 μm (similar to the basking shark tail surface), and therefore covers much of the roughness range of biological shark skin. Human hand skin has a typical roughness of 6.6 μm which is similar to that of thresher shark tails.

Golf balls have often been used to illustrate the effect of surface texture on drag (Alam et al., 2011; Bearman and Harvey, 1976), and we measured their three-dimensional surface characteristics for comparison to swimsuit and shark skin data (Supplemental Table S1). The relatively large surface dimples on golf balls result in roughness values of 85 – 115 μm, which is somewhat less than current 3D printed biomimetic shark skin.

References

Alam F., Steiner T., Chowdhury H., Moria H., Khan I., Aldawi F. & Subic A. (2011). A study of golf ball aerodynamic drag. *Procedia Engineering*, *13*, 226-231.

Bearman P. & Harvey J. (1976). Golf ball aerodynamics. *The Aeronautical Quarterly*, *27*, 112-122.

Bechert D. W., Bruse M. & Hage W. (2000). Experiments with three-dimensional riblets as an idealized model of shark skin. *Experiments in Fluids*, *28*, 403-412.

Dean B. & Bhushan B. (2010). Shark-skin surfaces for fluid-drag reduction in turbulent flow: a review. *Philosophical Transactions of the Royal Society A: Mathematical, Physical and Engineering Sciences*, *368*, 4775-4806.

Domel A. G., Domel G., Weaver J., Saadat M., Bertoldi K. & Lauder G. V. (2018a). Hydrodynamic properties of biomimetic shark skin: effect of denticle size and swimming speed. *Bioinspiration and Biomimetics*, *13*, 056014.

Domel A. G., Saadat M., Weaver J., Haj-Hariri H., Bertoldi K. & Lauder G. V. (2018b). Shark denticle-inspired designs for improved aerodynamics. *Journal of the Royal Society Interface*, *15*, 20170828.

Jung Y. C. & Bhushan B. (2010). Biomimetic structures for fluid drag reduction in laminar and turbulent flows. *Journal of Physics: Condensed Matter*, *22*, 035104.

Krieger K. 2004. Do pool sharks swim faster? : American Association for the Advancement of Science.

Lang A., Motta P., Habegger M. L., Hueter R. & Afroz F. (2011). Shark skin separation control mechanisms. *Marine Technology Society Journal*, *45*, 208-215.

Wen L., Weaver J. C. & Lauder G. V. (2014). Biomimetic shark skin: design, fabrication, and hydrodynamic function. *Journal of Experimental Biology*, *217*, 1656-1666.

Supplemental TABLE S1 Surface profilometry data from various materials for comparison to shark denticle data presented in Tables 1 – 3. Competition swimsuit materials are highlighted in bold. For comparison, the first two rows show data from mature thresher and white shark tails.

Material	Sq (μm)	Ssk	Sku	Sz (μm)	Isotropy	Texture direction 1 (°)
Common thresher (*Alopias vulpinus*)	5.6	-1.4	9.8	62.9	78	25
White shark (*Carcharodon carcharias*)	17.3	-0.51	3.8	143.7	NA	NA
Skin, back of human hand	6.6	-0.6	4.4	84.6	38.7	90.0
Sandpaper	3.2	-0.1	3.9	24.9	84.5	40.8
Polishing paper	12.2	-0.2	2.9	92.1	55.3	0.1
blueseventy® Fullbody Fastskin	3.6	0.3	3.2	32.1	70.1	63.6
TYR® Evictor	13.2	0.0	2.5	75.9	77.9	90.0
TYR® Venzo	13.8	-0.2	2.7	84.6	75.9	26.5
Speedo Lzr® LZR Racer Elite 2	15.9	0.1	2.6	88.9	68.7	42.3
Speedo Lzr® LZR X	22.0	-0.2	2.9	220	15.6	3.8
Speedo® FS Fastskin II	26.0	-0.4	3.2	161	6.83	0.1
Srixon Zstar® (golf ball)	85.0	-0.0	2.1	492	74.8	49.0
Callaway Hex® (golf ball)	115.0	-0.2	1.9	437	87.8	64.5

NA: isotropy and texture direction not measured for white shark tail surfaces.